RSC Advances

ROYAL SOCIETY OF CHEMISTRY

www.rsc.org/advances

A fluorescence on-off sensor for Cu^{2+} and its resultant complex as off-on sensor for Cr^{3+} in aqueous media

Yunling Gao[a*], Jieming Shu[a], Cong Zhang[a], Xiang Zhang[b], Haiyan Chen[c]**, Kejian Yao[a]*

[a] *State Key Laboratory Breeding Base of Green Chemistry Synthesis Technology, College of Chemical Engineering, Zhejiang University of Technology, Hangzhou 310032, China.*

[b] *School of Chemistry and Materials Science, Shanxi Normal University, Linfen 041004, China.*

[c] *Department of Biomedical Engineering, School of Life Science and Technology, State Key Laboratory of Natural Medicines, China Pharmaceutical University, Nanjing 210009, China.*

*Corresponding author: Tel: +86-571-88320951; Email address: gaoyl@zjut.edu.cn; yaokj@zjut.edu.cn

**Corresponding author: Tel: +86-25-83271080; Email address: chenhaiyan@cpu.edu.cn

Abstract

A new coumarin-quinoline based sensor **1** has been synthesized. The paramagnetic Cu^{2+} ion turned off the fluorescence of the sensor **1** with the 1:1 binding stoichometry. The resultant 1-Cu^{2+} complex in situ could act as an efficient "off-on" fluorescence sensor for the paramagnetic Cr^{3+} ion triggered by the 1:1 replacement of Cu^{2+} with Cr^{3+}. This selective fluorescence "on-off-on" sensor was used to identify Cu^{2+} and Cr^{3+} in living breast cancer MCF-7 cells using a confocal fluorescence microscopy, indicating that the sensor **1** has a potential application for the selective detection of Cu^{2+} and Cr^{3+} in living cells.

Keywords: Sensor; Copper; Chromium; Fluorescence; Cell imaging;

1. Introduction

Development of selective fluorescent chemosensors for detecting biologically or environmentally important metal ions is of great importance [1-3]. Serving as the third most abundant transition metal in the biological process, copper (II) has a key influence on copper-binding enzyme activities, including cytochrome c oxidase, catechol oxidase, amine oxidase and so on, both as a catalytic co-factor and as an allosteric component of cuproenzymes. Insufficient intake of Cu^{2+} often causes anemia, bone abnormality or neutropenia [4]. However, excessive accumulation of copper (II) is toxic to the human body and leads to oxidative stress and neurodegenerative diseases [5]. Consequently, developing fluorescent chemosensors of the selective recognition and quantification of Cu^{2+} is considerably significant in the biological and environmental process [6-14]. Trivalent chromium, as an essential micronutrient for humans, plays a critical role in preventing negatively affects in the metabolism of glucose and lipids, therefore chromium (III) deficiency may cause glucose and lipid metabolism disorder [15], resulting in diabetes and cardiovascular diseases, while a high concentration level of Cr^{3+} may cause genotoxic effect and destroy cellular structure [16]. Thus, the development of reliable, selective and sensitive fluorescent chemosensors for Cr^{3+} recognition has attracted immense interest in biological and environmental areas [17-22].

Recently, a variety of fluorescent chemosensors for the selective recognition of Cu^{2+} or Cr^{3+} have been reported which demonstrate high selectivities for the target Cu^{2+} or Cr^{3+} over other competitive metal ions based on the enhancement or quenching of fluorescence [16-22, 23-25], but most of them focus on single sensors for the selective recognition of only one target metal ion. Development of single sensors for the selective recognition of multiple metal ions, which would reduce analytic time, increase analysis speed and cut the cost, has received considerable attention.

Single chemosensors for the recognition of two metal ions have been reported, such as Fe^{3+}/Hg^{2+} [26], Zn^{2+}/Cu^{2+} [23-25], Zn^{2+}/Cd^{2+} [27-28], Zn^{2+}/Al^{3+} [29] and Hg^{2+}/Au^{3+} [30]. In contrast, single chemosensors to detect Cu^{2+}/Cr^{3+} are still rare.

In this study, we developed a coumarin-quinoline based sensor **1** (Scheme 1) for detecting of two metal ions Cu^{2+} and Cr^{3+} in aqueous media and living breast cancer MCF-7 cells. When the addition of excess Cu^{2+}, the sensor **1** undergone fluorescence quenching and a 10 nm red-shift of the maximum absorption wavelength. The 1:1 binding stoichometry was determined using the spectroscopic titration and Job's plot. The resultant 1-Cu^{2+} complex could detect the paramagnetic Cr^{3+} ion by fluorescence enhancement though 1:1 metal ion replacement approach. The sensor **1** showed excellent cell-membrane permeability and effectively distinguished Cu^{2+} and Cr^{3+} in living cells though fluorescence "on-off-on" signals.

2. **Materials and methods**

2.1 Instruments and reagents

All solvents and reagents were obtained from commercial sources (Sigma-Aldrich, TCI or Aladdin) and used without further purification. MCF-7 (breast cancer) cells used for the fluorescence imaging were purchased from American Type Culture Collection. Fluorescence spectra were recorded on a FluoroMax4 spectrometer with a set of excitation and emission slits both at 3.0 nm. Absorption spectra were recorded on a UV-2550 UV-vis spectrometer. FT-IR spectra were obtained on a Nicolet 6700 Fourier-transform infrared spectrometer. The pH titration was conducted on a Leici PHS-25 pH meter. NMR spectra were obtained on an AVANCE Ⅲ 500 MHz spectrometer with TMS as an internal standard. Mass spectra (MS) were recorded with an Accurate-Mass TOF LC/MS spectrometer. XPS were recorded on a Kratos AXIS Ultra DLD

spectrometer. The cells were imaged by an Olympus FV1100 laser confocal fluorescence microscopy.

2.2 UV-vis and fluorescence spectrometric determination

2.2.1 Preparation of test solutions for fluorescent studies

Stock solutions (1 mM) of nitrate salts of K^+, Ca^{2+}, Na^+, Mg^{2+}, Al^{3+}, Zn^{2+}, Fe^{3+}, Pb^{2+}, Hg^{2+}, Ag^+, Co^{2+}, Ni^{2+}, Cd^{2+}, Cu^{2+} and Cr^{3+} were prepared in ultrapure water. 1 mM of stock solution of the sensor **1** was prepared in DMSO. The test solution was prepared by appropriately diluting the stock solution of the sensor **1** to 0.1 M HEPES-DMSO (9:1, v/v, pH = 7.2) solution and then adding the appropriate amount of each metal ion stock solution. The fluorescence quantum yield was calculated using quinine sulfate (Φ = 0.51) in 0.5 M H_2SO_4 as the standard.

2.2.2 Calculation of the binding stoichometry and association constant

The binding stoichometry of the metal ion to the sensor **1** was determined using Job plot experiments [31]. The association constant (K_a) of the metal ion binding to the sensor **1** was determined from the fluorescence titration data based on the reported Benesi-Hildebrand equation [32-33].

2.3 Quantum chemical calculation

Quantum chemical calculations were performed using Gaussian 09 program [34]. The ground state structure of the sensor **1** was optimized based on density functional theory (DFT) using B3LYP functional [35-36] and 6-311G(d,p) basis set. Frequency calculations were carried out on all optimized geometries to ensure that the obtained structures represent local minima without imaginary frequencies. Time-dependent (TD) DFT calculations were also performed using the same basis set as those in the geometry optimization.

2.4 Cell culture and fluorescence imaging

The cell lines were cultured in RPMI-1640 medium supplemented with 10% (v/v) calf serum, penicillin (100 U mL^{-1}), and streptomycin (100 mg mL^{-1}). The cells were maintained at 37 ^{0}C in a humidified atmosphere containing 5% CO_2.

To investigate the influence of Cu^{2+} and Cr^{3+} on the fluorescence intensity of the sensor **1** in cell level, MCF-7 cells were seeded in 12 laser confocal fluorescence microscopy culture dishes with a density of 3×10^5 cells/well and subsequently incubated at 37 ^{0}C. After 24 h of cell attachment, the 12 dishes were separated into 4 groups randomly. The cells in first group without treatment with any samples were utilized as the contrast. The cells in the second group were treated with 40 μL of the sensor **1** (10 μM) in a HEPES-DMSO (9:1) solution and then incubated for 30 min at 37 ^{0}C. Phosphate-buffered saline (PBS) was utilized to wash the cells for three times. Following the experimental steps for the second group, the cells in the third group were incubated with 20 μL of the Cu^{2+} solution (30 μM) for 30 min at 37 ^{0}C. The cells in the fourth group were further treated with 20 μL of the Cr^{3+} solution (30 μM) for 30 min at 37 ^{0}C. After washing three times with PBS, the cells were imaged using a laser confocal fluorescence microscopy.

*2.5 Synthesis of the sensor **1***

7-diethylaminocoumarin-3-carboxylic acid (10 mmol, 2.61 g) and 8-aminoquinoline (10 mmol, 1.44 g) were dissolved in 100 mL chloroform including dicyclohexyl carbodiimide (10 mmol, 2.06 g) and 4-dimethylaminopyridine (50 mg). The solution was stirred for 6 hours at room temperature, and then the white precipitate dicyclohexylurea was filtered to obtain the clarified yellow solution which was extracted with water three times and dried with anhydrous sodium sulfate. Subsequently, the solvent was removed using the rotary evaporation to obtain a crude product which was further

purified by the silica gel column chromatography (ethyl acetate: dichloromethane = 1:10, v/v) to give **1** as a yellow solid in 61.5% yield. m.p. 222.5-224.3 ^{0}C ; ^{1}HNMR (500 MHz, $CDCl_3$): δ 1.25 (t, 6H, J = 7.2 Hz, -CH_3), 3.47 (q, 4H, J = 7.2 Hz, -CH_2-), 6.55 (s, 1H, Ar-H), 6.67 (d, 1H, J = 9.0 Hz, Ar-H), 7.45-7.48 (m, 2H, Ar-H), 7.53-7.59 (m, 2H, Ar-H), 8.17 (d, 1H, J = 8.25 Hz, Ar-H), 8.84 (s, 1H, Ar-H), 8.99-9.01 (m, 2H, Ar-H), 12.76 (s, 1H, N-H); ^{13}CNMR (125 MHz, $CDCl_3$): δ 162.5, 161.6, 157.9, 152.7, 148.9, 148.4, 139.6, 136.1, 135.6, 131.2, 128.1, 127.2, 121.9, 121.5, 117.7, 111.1, 109.9, 108.6, 96.8, 45.1, 12.5; FTIR (cm^{-1}) 2971.5, 2925.2, 1710.9, 1650.5, 1612.8, 1570.7, 1506.9, 1420.7, 1350.2, 1263.4, 1188.3, 1133.7, 1076.9, 821.5, 788.6; HRMS calcd 388.1661, found 388.1657.

3. Results and discussion

*3.1 Synthesis and characterization of the sensor **1***

The sensor **1** was obtained by the reaction of 7-diethylaminocoumarin-3-carboxylic acid and 8-aminoquinoline where a new amide bond was formed between the coumarin and quinoline moiety (Scheme 1). To elucidate the structure of the sensor **1**, the DFT calculations were carried out and the lowest energy structure of the sensor **1** is presented in Fig. 1. The sensor **1** forms a large coplanar structure over quinoline and coumarin moieties and shows a cis conformer though the amide bond. In addition, the shortened N_{amine}-C bond length (1.37516 Å) and C_{alkyl}-N_{amine}-C_{alkyl} or C_{aryl}-N_{amine}-C_{aryl} angle of almost 120° suggest the lone pairs of amine N are delocalized and a p-π conjugated system is hence formed. Consequently, the sensor **1** presents a greater π conjugate system of electronic delocalization than its precursor coumarin.

The synthesized yellow compound shows a maximum absorption band at 445 nm which undergoes a red-shift compared to its precursor [37], indicating a greater electronic delocalization

effect on the sensor **1** in good agreement with the above DFT-data. TD-DFT calculations predict that the experimentally observed maximum absorption band at 445 nm is predominately originating from the HOMO to LUMO transition (Fig. 1), where the HOMO delocalizes over the entire π system, whereas the LUMO has a significant contribution from the coumairn moiety. Accordingly, the maximum absorption of the sensor **1** presents a charge transfer π-π* transition from the occupied quinoline to unoccupied coumarin orbitals, which may cause the red shift of the absorption band. The quantum yield of the sensor **1** was 0.109 determined in a HEPES-DMSO buffer solution (0.1 M) with the emission band at 491 nm (Fig. 2).

3.2 Spectroscopic properties

The recognition ability of the sensor **1** was obtained by mixing it with various metal ions including K^+, Ca^{2+}, Na^+, Mg^{2+}, Al^{3+}, Zn^{2+}, Fe^{3+}, Pb^{2+}, Hg^{2+}, Ag^+, Co^{2+}, Ni^{2+}, Cd^{2+}, Cu^{2+} and Cr^{3+} in aqueous solution using the fluorescence and UV-vis spectrophotometric titration. When excited at 437 nm, only Cu^{2+} caused a significant quenching (Φ = 0.024) in the fluorescence intensity of the sensor **1** which could be attributed to the coordination of the paramagnetic Cu^{2+} ions (Fig. 2). Upon incremental addition of Cu^{2+}, the fluorescence intensity at 491 nm decreased gradually and then reached the minimum after adding 5 equivalents of Cu^{2+} (Fig. 3). The linear relationship of the fluorescence titration (Fig. 3) and Job's plot (Fig. 4) suggest the stoichiometric ratio of the sensor **1** with Cu^{2+} appears to be 1 to 1. The association constant K_a of the sensor **1** for Cu^{2+} was 3.65×10^3 M^{-1} (Fig. S1) and the detection limit of the sensor **1** for Cu^{2+} was 2.5 μM which was reasonable for the detection of the copper ion in the blood (15.7-23.6 μM) [38-39] and drinking water (~30 μM) [40]. After binding with Cu^{2+}, the absorbance at 445 nm increased and the maximum absorption band was shifted to 455 nm which led the color change from light yellow to yellow (Fig. 5 and Fig.

S2). The fluorescence changes of the sensor **1** in the absence and presence of Cu^{2+} in different pH values were evaluated. As shown in Fig. S3, Cu^{2+} caused the fluorescence quenching over a wide pH range of 4.5-7.5. This indicates that the sensor **1** can be potentially applicable as a selective sensor for Cu^{2+} in near neutral and acidic medium, which is promising in both the environmental and biological application.

To further explore the influence of other metal ions on the 1-Cu^{2+} complex, the competitive experiments were carried out with other metal ions (30 μM) in the presence of Cu^{2+} (30 μM) and the sensor **1** (10 μM) (Fig. S4). The observed fluorescence spectra of K^{+}, Ca^{2+}, Na^{+}, Mg^{2+}, Al^{3+}, Zn^{2+}, Fe^{3+}, Pb^{2+}, Hg^{2+}, Ag^{+}, Co^{2+}, Ni^{2+} and Cd^{2+} in the presence of the 1-Cu^{2+} complex were similar to that caused with the 1-Cu^{2+} complex alone. Attractively, the addition of Cr^{3+} caused a 3.8-fold enhancement of the fluorescence intensity of the 1-Cu^{2+} complex (Fig. 6-7 and Fig. S5). The quantum yield of the emission band was increased to 0.064.

Fluorescence titration experiments were performed to further evaluate the sensing ability of 1-Cu^{2+} (10 μM) to Cr^{3+} (Fig. 8). The fluorescence intensity of the 1-Cu^{2+} solution increased gradually with the addition of Cr^{3+} and remained fairly constant until 3.0 equivalents of Cr^{3+} were added. According to the Benesi-Hildebrand equation, the association constant of 1-Cu^{2+} with Cr^{3+} was calculated to be 5.4×10^{4} M^{-1} from the fluorescence titration curve (Fig. S6). The association constant of 1-Cu^{2+} for Cr^{3+} is 3.9-fold of that for the sensor **1** with Cu^{2+}, suggesting the increased fluorescence may originate from the replacement of Cu^{2+} by Cr^{3+}. The linear relationship of the fluorescence titration of 1-Cu^{2+} also indicated a 1:1 binding mode for 1-Cu^{2+} with Cr^{3+} which was further supported by the UV-vis titration of Cr^{3+} to 1-Cu^{2+} (Fig. S7). The above observations suggest that Cu^{2+} in the 1-Cu^{2+} complex could be replaced by only Cr^{3+}, indicating the 1-Cu^{2+}

complex has a good selectivity for Cr^{3+} and could be an efficient "off-on" sensor for Cr^{3+}. A schematic for the analysis of the mixed metal ions using the sensor **1** is shown in Scheme 2. When the resultant 1-Cu^{2+} complex in situ is used to as the sensor, existence of Cr^{3+} would turn on the fluorescence of the 1-Cu^{2+} complex. In contrast, other metal ions including Cu^{2+} would have no obvious influence on the fluorescence intensity of the 1-Cu^{2+} complex. The sensor **1** can detect the Cu^{2+} ion from the solution of the mixed metal ions without Cr^{3+} based on the fluorescence quenching.

3.3 Possible sensing mechanism

To get insight of the binding mode of the sensor **1** with Cu^{2+}, IR, NMR and MS were first employed. IR spectra of the sensor **1** and 1-Cu^{2+} are shown in Fig. 9. The sensor **1** exhibits a band of the medium intensity at around 3440 cm^{-1}. This band can be assigned to *v* NH which is also be observed in the spectrum of 1-Cu^{2+}. Two bands appearing at 1701.9 and 1650.5 cm^{-1} are the C=O stretching vibration of the ester carbonyl and amide carbonyl groups, respectively. In the spectrum of 1-Cu^{2+}, the C=O vibration band of the ester carbonyl is shifted to the lower frequency by 48 cm^{-1} suggesting the binding of the oxygen of the ester carbonyl group with Cu^{2+}, whereas there are not obvious differences in the C=O stretching band of the amide carbonyl group before and after the addition of Cu^{2+}.

The ^{1}HNMR spectrum of the sensor **1** with the addition of Cu^{2+} reveals that the amide hydrogen (NH) at 12.6 ppm (Fig. S8) is still held which is in good agreement with the IR observation. Due to the paramagnetic Cu^{2+} ion, the signals of ^{1}HNMR are broadened and hence distinct shifts of proton signals are not observed. As discussed above, the formation of 1-Cu^{2+} is further confirmed using HRMS (Fig. S9) where the peak at m/z 449.0808 corresponds to $[1\text{-Cu-H}]^+$

and moreover a peak at m/z 527.0953 corresponding to $[1\text{-}Cu+DMSO-H]^+$ is also observed, indicating one solvent involves in the coordination to $1\text{-}Cu^{2+}$.

To more clearly understand the structure of $1\text{-}Cu^{2+}$, XPS spectra were carried out and the standard samples, coumarin 120 and 8-aminoquinoline, were also analyzed using XPS to help further assign the O and N groups. The results are presented in Fig. S10 and the corresponding assignments are listed in Table 1. When Cu^{2+} is bound to the sensor **1**, the binding energy of the oxygen of the ester carbonyl group in the sensor **1** (528.33 eV) is shifted to the higher energy by 0.6 eV, while those of nitrogen atoms of amide and aromatic groups undergo the lower energy shift by 0.55 eV and 0.19 eV in $1\text{-}Cu^{2+}$, respectively, which suggest these atoms have involved in the coordination to Cu^{2+}, in good agreement with the above IR and NMR analyses.

Based on the analysis of the fluorescence and UV-vis titration, Job's plot, IR, NMR, HRMS and XPS, the possible binding mode of the sensor **1** with Cu^{2+} in solvent media is proposed as shown in Fig. 10, where a four-coordination copper(II) complex is formed with three coordination sites in the sensor **1** and one coordination site from the solvent.

To explore the possible mechanism of the fluorescence recovery of the $1\text{-}Cu^{2+}$ complex after the addition of Cr^{3+}, NMR and IR were also carried out as presented in Fig. S8 and S11. Similar to the ^{1}HNMR spectrum of $1\text{-}Cu^{2+}$, the paramagnetic Cr^{3+} ion also causes the broader proton signals, hence no significant shifts of proton signals are observed with the held amide hydrogen at 12.6 ppm. Different from the IR characteristics of the $1\text{-}Cu^{2+}$ complex, IR spectrum of $1\text{-}Cu^{2+}$ with Cr^{3+} shows that the C=O stretching vibration of the ester carbonyl group in the ligand is shifted back from ca. 1650 cm^{-1} to ca. 1700 cm^{-1} which distinctly suggests that copper (II) may be replaced by chromium (III). In addition, individual chromium (III) ions were also added to the sensor **1** and its IR spectrum

shows the same band at ca. 1700 cm^{-1} which can be assigned as the C=O stretching vibration of the ester carbonyl group in the ligand. The above observations indicate that the oxygen of the ester carbonyl group in the ligand may not participate in the coordination to chromium (III). IR spectra of 1-Cr^{3+} and 1-Cu^{2+} in DMSO were also recorded and shown in Fig S11 where the bands of NO_3 in 1-Cr^{3+} complex are different from those in 1-Cu^{2+} complex with three bands at ca. 1437, 1408, 1318 cm^{-1} *vs* ca. 1350 cm^{-1} for 1-Cr^{3+} and 1-Cu^{2+}, respectively. As the analysis for the four-coordination 1-Cu^{2+} complex in the solution, one solvent with the sensor **1** is bound with copper (II) with the free NO_3 groups in good agreement with its IR observation in DMSO, whereas NO_3 groups may involve in the binding with chromium (III) in 1-Cr^{3+}.

Overall, referring to the analysis of the fluorescence, UV-vis titration and the larger association constant of 1-Cu^{2+} for Cr^{3+} *vs* the sensor **1** for Cu^{2+}, the possible sensing mechanism in solvent media is proposed that Cr^{3+} replaced Cu^{2+} and then was bound to the sensor **1** as shown in Fig. 10.

3.4 Living cell imaging

To further demonstrate the practical application of the sensor **1** for the detection of Cu^{2+} and Cr^{3+} in biological samples, the fluorescence imaging was carried out in MCF-7 breast cancer living cells as showed in Fig 11. MCF-7 cells themselves have not showed obvious fluorescence. When the cells were treated with 10 μM of the sensor **1** for 30 min at 37 ^{0}C, the intracellular bright green fluorescence was observed in MCF-7 cells. Subsequently, upon treating above cells with an excessive amount of Cu^{2+} (30 μM) for 30 min at 37 ^{0}C, the fluorescence intensity in MCF-7 cells was significantly quenched. Finally, when 30 μM of the Cr^{3+} solution was further added, the intracellular fluorescence was easily recovered and showed a green fluorescence imaging. The bright field images also confirmed that cells were visible before and after the addition of the sensor

1, Cu^{2+} and Cr^{3+}. These results indicate that the sensor **1** has excellent cell-membrane permeability. Moreover, the sensor **1** is applicable for the recognition of Cu^{2+} and Cr^{3+} in living cells.

4 Conclusion

In conclusion, a new fluorescence sensor **1** has been synthesized, which showed the selective recognition for Cu^{2+} by fluorescence quenching. The resultant 1-Cu^{2+} complex can serve as a fluorescent turn-on sensor for Cr^{3+} via the replacement of Cu^{2+}. The binding mode of the sensor **1** with Cu^{2+} or Cr^{3+} was 1:1 to form the four-coordination 1-Cu^{2+} complex or six-coordination 1-Cr^{3+} complex.

This "on-off-on" switching sensor was successfully applied in the live cell fluorescence imaging and therefore further demonstrates its greatly potential applicability for the recognition of Cu^{2+} and Cr^{3+} in living cells.

Acknowledgements

Our work was supported by Zhejiang Provincial Natural Science Foundation of China (Grant No. LY15B070004 and LY12B07010) and National Natural Science Foundation of China (Grant No. 20807037 and 81371684).

Supplementary data

NMR spectra, FT-IR spectra and XPS spectra; Benesi-Hildebrand plot; pH titration curves; UV-vis and fluorescence spectra and DFT-optimized structure.

References

[1] Y. Jeong, J. Yoon, Recent progress on fluorescent chemosensors for metal ions, Inorganica Chimica Acta, 2012, 381, 2–14.

[2] L. Prodi, F. Bolletta, M. Montalti, N. Zaccheroni, Luminescent chemosensors for transition

metal ions, Coordination Chemistry Reviews, 2000, 205, 59–83.

[3] J. Du, M. Hu, J. Fan, X. Peng, Fluorescent chemodosimeters using “mild” chemical events for the detection of small anions and cations in biological and environmental media, Chemical Society Reviews, 2012, 41, 4511–4535.

[4] R. Uauy, M. Olivares, M. Gonzalez, Essentiality of copper in humans, The American Journal of Clinical Nutrition, 1998, 67, 952S–959S.

[5] K. J. Barnham, C. L. Masters, A. I. Bush, Neurodegenerative diseases and oxidative stress, Nature Reviews Drug Discovery, 2004, 3, 205–214.

[6] S. P. Wu, T. H. Wang, S. R. Liu, A highly selective turn–on fluorescent chemosensor for copper(II) ion, Tetrahedron, 2010, 66, 9655–9658.

[7] N. Aksuner, E. Henden, I. Yilmaz, A. Cukurovali, A highly sensitive and selective fluorescent sensor for the determination of copper(II) based on a schiff base, Dyes and Pigments, 2009, 83, 211–217.

[8] X. R. He, H. B. Liu, Y. L. Li, S. Wang, Y.J.Li, N. Wang, J. C. Xiao, X. Xun, D. B. Zhu, Gold Nanoparticle‐Based Fluorometric and Colorimetric Sensing of Copper (II) Ions. Advanced Materials, 2005, 17, 2811-2815.

[9] S. Pu, L. Ma, G. Liu, H. Ding, B. Chen, A multiple switching diarylethene with a phenyl-linked rhodamine B unit and its application as chemosensor for Cu^{2+}. Dyes and Pigments, 2015, 113, 70-77.

[10] H. F. Wang, S. P. Wu, A pyrene–based highly selective turn–on fluorescent sensor for copper(II) ions and its application in living cell imaging, Sensors and Actuators B:Chemical, 2013, 181, 743–748.

[11] M. Xu, C. Yin, F. Huo, Y. Zhang, J. Chao, A highly sensitive "ON–OFF–ON" fluorescent probe with three binding sites to sense copper ion and its application for cell imaging, Sensors and Actuators B: Chemical, 2014, 204, 18-23.

[12] A. Kumar, V. Kumar, U. Diwan, K. K. Upadhyay, Highly sensitive and selective naked–eye detection of Cu^{2+} in aqueous medium by a ninhydrin–quinoxaline derivative, Sensors and Actuators B:Chemical, 2013, 176, 420–427.

[13] A. Kumar, V. Vanita, A. Walia, S. Kumar, N,N–dimethylaminoethylaminoanthrone A chromofluorogenic chemosensor for estimation of Cu^{2+} in aqueous medium and HeLa cells imaging, Sensors and Actuators B:Chemical, 2013, 177, 904–912.

[14] X. Q. Chen, M. J. Jou, H. Lee, S. Z. Kou, J. Lim, S. W. Nam, S. Park, K. M. Kim, J. Yoon , New fluorescent and colorimetric chemosensors bearing rhodamine and binaphthyl groups for the detection of Cu^{2+}, Sensors and Actuators B:Chemical, 2009, 137, 597–602.

[15] M. Zayed, T. Norman, Chromium in the environment: factors affecting biological remediation, Plant and Soil, 2003, 249, 139–156.

[16] S. A. Katz, H. Salem, The biological and environmental chemistry of chromium; VCH Publishers: New York, 1994.

[17] S. Samanta, S. Goswami, A. Ramesh, G. Das, A new fluorogenic probe for solution and intra–cellular sensing of trivalent cations in model human cells, Sensors and Actuators B: Chemical, 2014, 194, 120–126.

[18] S. Wu, K. Zhang, Y. Wang, D. Mao, X. Liu, J. Yu, L. Wang, A novel Cr^{3+} turn–on probe based on naphthalimide and BINOL framework, Tetrahedron Letters, 2014, 55, 351–353.

[19] P. Xie, F. Guo, Y. Xiao, Q. Jin, D. Yao, Z. Huang, A fluorescent chemosensor based on

rhodamine for Cr^{3+} in red spectral region in aqueous solutions and living cells, Journal of Luminescence, 2013, 140, 45–50.

[20] M. Wang, J. Wang, W. Xue, A. Wu, A benzimidazole–based ratiometric fluorescent sensor for Cr^{3+} and Fe^{3+} in aqueous solution, Dyes and Pigments, 2013, 97, 475–480.

[21] F. Hu, B. Zheng, D. Wang, M. Liu, J. Du, D. Xiao, A novel dual–switch fluorescent probe for Cr(III) ion based on PET–FRET processes, The Analyst, 2014, 139, 3607–3613.

[22] J. G. Zhang, L. Zhang, Y. L. Wei, J. B. Chao, S. B. Wang, S. M. Shuang, Z. W. Cai, C. Dong, A selective carbazole–based fluorescent probe for chromium(III), Analytical Methods, 2013, 5, 5549–5554.

[23] L. Tang, J. Zhao, M. Cai, P. Zhou, K. Zhong, S. Hou, Y. Bian, An e^{ff}icient ^{se}nsor ^{f}or rela^{y} recognition of Zn^{2+} and Cu^{2+} through fluorescence 'off–on–off' functionality, Tetrahedron Letters, 2013, 54, 6105–6109.

[24] Y. M. Liu, Q. Fei, H. Y. Shan, M. H. Cui, Q. Liu, G. D. Feng, Y. F. Huan, A novel fluorescent 'off–on–off' probe for relay recognition of Zn^{2+} and Cu^{2+} derived from N,N–bis(2–pyridylmethyl)amine, The Analyst, 2014, 139, 1868–1875.

[25] Z. Li L., Zhang, L. Wang, Y. Guo, L. Cai, M. Yu, L. Wei, Highly sensitive and selective fluorescent sensor for Zn^{2+}/Cu^{2+} and new approach for sensing Cu^{2+} by central metal displacement, Chemical Communications, 2011, 47, 5798–5800.

[26] Y. Y. Yan, Z. P. Che, X. Yu, X. Y. Zhi, J. J. Wang, H. Xu, Fluorescence 'on–off–on' chemosensor for sequential recognition of Fe^{3+} and Hg^{2+} in water based on tetraphenylethylene motif, Bioorg anic&Medicinal Chemistry, 2013, 21, 508–513.

[27] L. Xue, Q. Liu, H. Jiang, Ratiometric Zn^{2+} fluorescent sensor and new approach for sensing

Cd^{2+} by ratiometric displacement,Organic letters, 2009, 11, 3454–3457.

[28] J. Wang, W. Lin, W. Li, Single fluorescent probe displays a distinct response to Zn^{2+} and Cd^{2+}, Chemistry–A European Journal, 2012, 18, 13629–13632.

[29] D. Maity, T. Govindaraju, A differentially selective sensor with fluorescence turn–on response to Zn^{2+} and dual–mode ratiometric response to Al^{3+} in aqueous media. Chemical Communications, 2012, 48, 1039–1041.

[30] E. Karakuş, M. Üçüncü, M. Emrullahoğlu, A rhodamine/BODIPY–based fluorescent probe for the differential detection of Hg (II) and Au (III), Chemical Communications, 2014, 50, 1119–1121.

[31] A. Senthilvelan, I. Ho, K. C. Chang, G. H. Lee, Y. H. Liu, W. S. Chung, Cooperative recognition of a copper cation and cnion by a calix [4] arene substituted at the lower rim by a β‐amino□α, β□unsaturated ketone, Chemistry‐A European Journal, 2009, 15, 6152–6160.

[32] H. A. Benesi, J. H. Hildebrand, A spectrophotometric investigation of the interaction of iodine with aromatic hydrocarbons, Journal of the American Chemical Society, 1949, 71, 2703–2707.

[33] R. B. Singh, S. Mahanta, N. Guchhait, Spectral modulation of charge transfer fluorescence probe encapsulated inside aqueous and non–aqueous β–cyclodextrin nanocavities. Journal of Molecular Structure, 2010, 963, 92–97.

[34] M. J. Frisch, G.W. Trucks, H.B. Schlegel, G.E. Scuseria, M.A. Robb, J.R. Cheeseman, G. Scalmani, V. Barone, B. Mennucci, G.A. Petersson, H. Nakatsuji, M. Caricato, X. Li, H.P. Hratchian, A.F. Izmaylov, J. Bloino, G. Zheng, J.L. Sonnenberg, M. Hada, M. Ehara, K. Toyota, R. Fukuda, J. Hasegawa, M. Ishida, T. Nakajima, Y. Honda, O. Kitao, H. Nakai, T. Vreven, J.A. Montgomery Jr., J.E. Peralta, F. Ogliaro, M. Bearpark, J.J. Heyd, E. Brothers, K.N. Kudin, V.N.

Staroverov, R. Kobayashi, J. Normand, K. Raghavachari, A. Rendell, J.C. Burant, S.S. Iyengar, J. Tomasi, M. Cossi, N. Rega, J.M. Millam, M. Klene, J.E. Knox, J.B. Cross, V. Bakken, C. Adamo, J. Jaramillo, R. Gomperts, R.E. Stratmann, O. Yazyev, A.J. Austin, R. Cammi, C. Pomelli, J.W. Ochterski, R.L. Martin, K. Morokuma, V.G. Zakrzewski, G.A. Voth, P. Salvador, J.J. Dannenberg, S. Dapprich, A.D. Daniels, O. Farkas, J.B. Foresman, J.V. Ortiz, J. Cioslowski, D.J. Fox, Gaussian 09, Gaussian Inc., Wallingford, CT 2009.

[35] A. D. Becke, Density–functional exchange–energy approximation with correct asymptotic behavior, Physical Review A, 1988, 38, 3098–3100.

[36] J. P. Perdew, Density functional approximation for the correlation energy of the inhomogeneous electron gas, Physical Review B, 1986, 33, 8822–8824.

[37] H. Zhang, T. Yu, Y. Zhao, D. Fan, L. Chen, Y. Qiu, C. Yang, Crystal structure and photoluminescence of 7–(N,N′–diethylamino)–coumarin–3–carboxylic acid, Spectrochimica Acta Part A: Molecular and Biomolecular Spectroscopy, 2008, 69, 1136–1139.

[38] J. Wang, L. Long, D. Xie, X. Song, Cu^{2+}–selective "Off–On" chemsensor based on the rhodamine derivative bearing 8–hydroxyquinoline moiety and its application in live cell imaging. Sensors and Actuators B: Chemical, 2013, 177, 27–33.

[39] H. S. Jung, P. S. Kwon, J. S. Kim, C. S. Hong, J.W. Kim, S. Yan, J. Y. Lee, J. H. Lee, T. Joo, J. S. Kim, Coumarin–derived Cu^{2+}–selective fluorescence sensor: synthesis, mechanisms, and applications in living cells, Journal of the American Chemical Society, 2009, 131, 2008–2012.

[40] T. G. Jo, Y. J. Na, J. J Lee, M. M. Lee, S. Y. Lee, C. Kim, A diaminomaleonitrile based selective colorimetric chemosensor for copper(II) and fluoride ions, New Journal of Chemistry, 2015, 39, 2580-2587.

Figure and scheme captions

Table 1. XPS results of the sensor **1** and 1-Cu^{2+}. Asterisk (*) presents the assigned atom.

Scheme 1. Synthesis of the sensor **1**.

Scheme 2. Schematic for the analysis of the mixed metal ions using the sensor **1**.

Fig. 1. The optimized geometry (left) and significant frontier molecular orbitals (right) of the sensor **1** using B3LYP functional and 6-311G(d,p) basis set (blue atom, N; red atom, O).

Fig. 2. (a) Fluorescence changes of the sensor **1** (10 μM) upon addition of 3.0 equiv. of individual metal ions in 0.1 M HEPES-DMSO (9:1, v/v, pH = 7.2) solution. (b) The relative fluorescent intensity of I_0/I at 491 nm, where I_0 and I are the fluorescent intensity of the sensor **1** (10 μM) in the absence and presence of metal ions, respectively. Inset: a picture of fluorescence changes of the sensor **1** (10 μM) upon addition of 3.0 equiv. of individual metal ions in 0.1 M HEPES-DMSO (9:1, v/v, pH = 7.2) solution.

Fig. 3. Fluorescence response of the sensor **1** (10 μM) to different equivalents of Cu^{2+} (0, 0.2, 0.5, 0.8, 1.0, 1.5, 2.0, 2.5, 3.0, 3.5, 4.0, 4.5, 5.0 equiv.) in 0.1 M HEPES-DMSO (9:1, v/v, pH = 7.2) solution.

Fig. 4. Job's plot for the sensor **1** *vs* Cu^{2+} in 0.1 M HEPES-DMSO (9:1, v/v, pH = 7.2) solution. The total concentration of the sensor **1** and Cu^{2+} was 30 μM.

Fig. 5. Absorption changes of the sensor **1** (10 μM) upon addition of 3.0 equiv. of individual metal ions in 0.1 M HEPES-DMSO (9:1, v/v, pH = 7.2) solution; Inset: a picture of absorption changes of the sensor **1** (10 μM) upon addition of 3.0 equiv. of individual metal ions in 0.1 M HEPES-DMSO (9:1, v/v, pH = 7.2) solution.

Fig. 6. Fluorescence response of the sensor **1** (10 μM) and Cu^{2+} (30 μM) in the presence of other different metal ions (30 μM) in 0.1 M HEPES-DMSO (9:1, v/v, pH = 7.2) solution.

Fig. 7. Fluorescence response of the sensor **1** (10 μM) and Cu^{2+} (30 μM) in the presence of other different metal ions (30 μM) in 0.1 M HEPES-DMSO (9:1, v/v, pH = 7.2) solution.

Fig. 8. Fluorescence changes of 1-Cu^{2+} (10 μM) on addition of different equivalents of Cr^{3+} in 0.1 M HEPES-DMSO (9:1, v/v, pH = 7.2) solution. Inset: the fluorescence intensity of 1-Cu^{2+} (10 μM) at 491 nm as a function of equivalents of Cr^{3+} in 0.1M HEPES-DMSO (9:1, v/v, pH = 7.2) solution.

Fig. 9. FT-IR spectra of the sensor **1** and **1**-Cu^{2+} with the KBR compression method.

Fig. 10. Possible sensing mechanism of the sensor **1** for the sequential recognition of Cu^{2+} and Cr^{3+}.

Fig.11. Confocal fluorescence images in MCF-7 cells. (a) cells untreated with any samples as blank test; (b) cells incubated with 10 μM of the sensor **1** for 30 min at 37 ^{0}C; (c) cells further incubated with 30 μM of the Cu^{2+} solution for another 30 min at 37 ^{0}C; (d) cells incubated with 10 μM of the sensor **1** and 30 μM of the Cu^{2+} solution, and further incubated with 30 μM of the Cr^{3+} solution for 30 min at 37 ^{0}C; (e) bright field image of cells in panel a; (f) bright field image of cells in panel b; (g) bright field image of cells in panel c; (h) bright field image of cells in panel d.

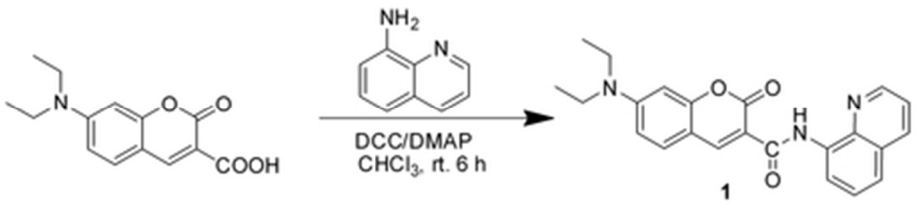

Scheme 1. Synthesis of the sensor 1.
38x8mm (300 x 300 DPI)

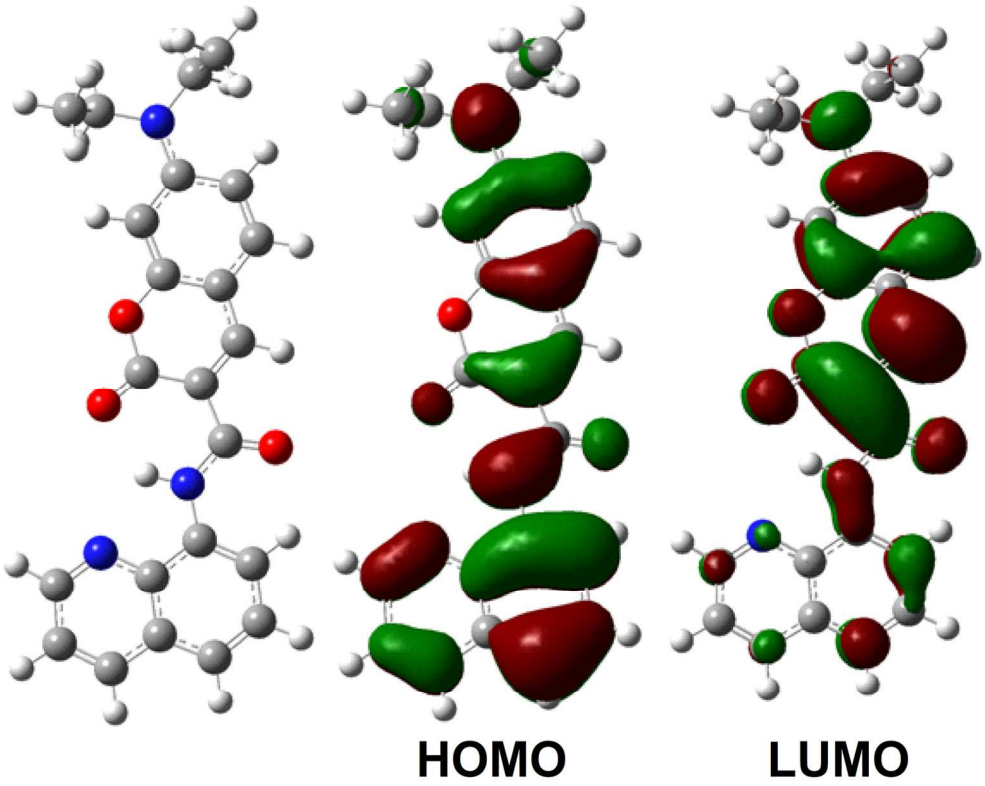

Fig. 1. The optimized geometry (left) and significant frontier molecular orbitals (right) of the sensor 1 using B3LYP functional and 6-311G(d,p) basis set (blue atom, N; red atom, O).
136x110mm (300 x 300 DPI)

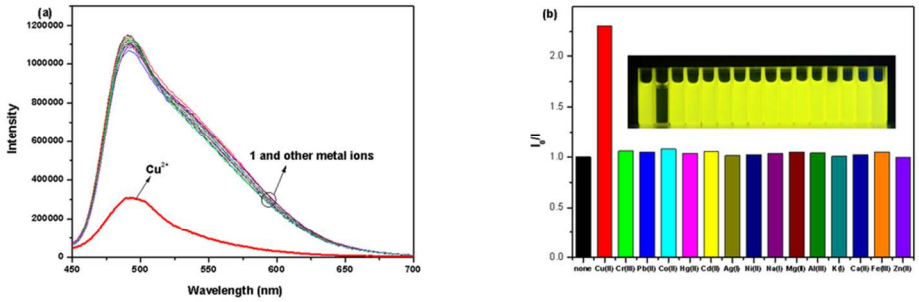

Fig. 2. (a) Fluorescence changes of the sensor 1 (10 μM) upon addition of 3.0 equiv. of individual metal ions in 0.1 M HEPES-DMSO (9:1, v/v, pH = 7.2) solution. (b) The relative fluorescent intensity of I0/I at 491 nm, where I0 and I are the fluorescent intensity of the sensor 1 (10 μM) in the absence and presence of metal ions, respectively. Inset: a picture of fluorescence changes of the sensor 1 (10 μM) upon addition of 3.0 equiv. of individual metal ions in 0.1 M HEPES-DMSO (9:1, v/v, pH = 7.2) solution.
44x16mm (600 x 600 DPI)

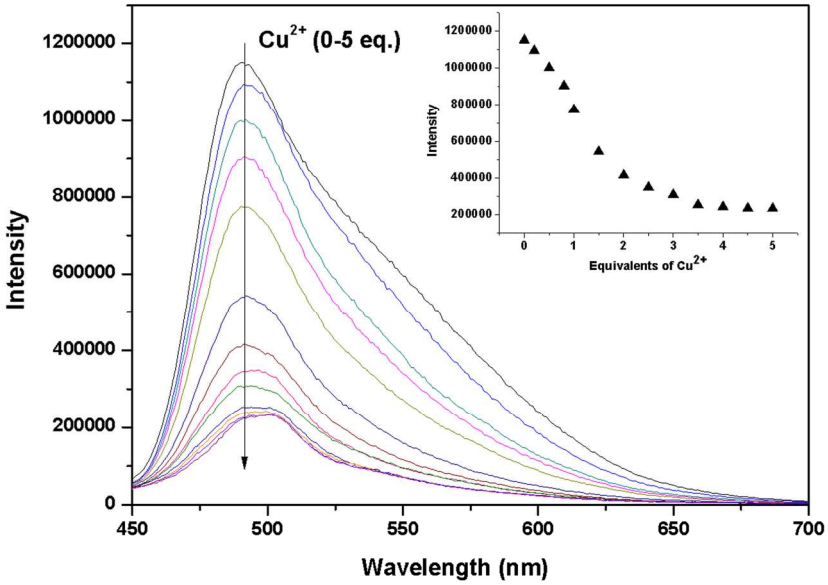

Fig. 3. Fluorescence response of the sensor 1 (10 μM) to different equivalents of Cu2+ (0, 0.2, 0.5, 0.8, 1.0, 1.5, 2.0, 2.5, 3.0, 3.5, 4.0, 4.5, 5.0 equiv.) in 0.1 M HEPES-DMSO (9:1, v/v, pH = 7.2) solution.
85x60mm (600 x 600 DPI)

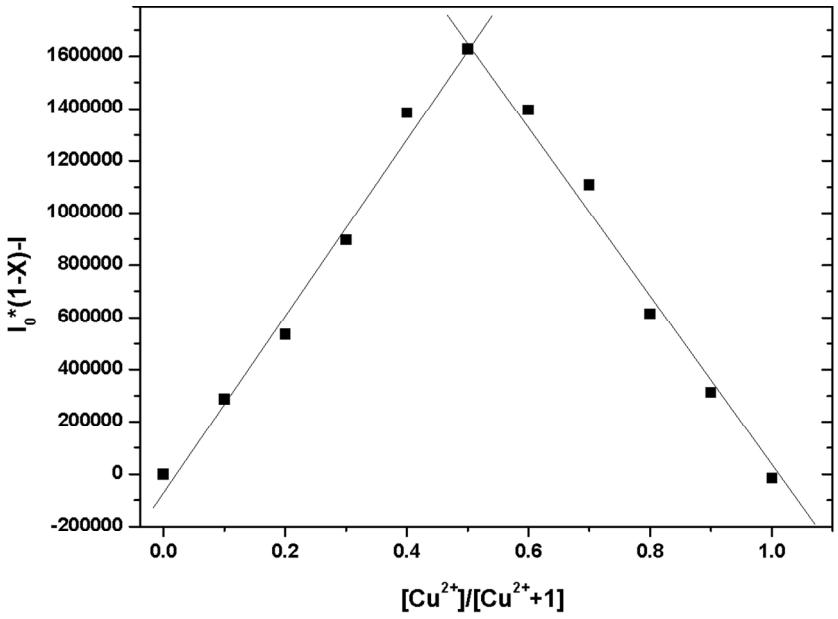

Fig. 4. Job's plot for the sensor 1 vs Cu2+ in 0.1 M HEPES-DMSO (9:1, v/v, pH = 7.2) solution. The total concentration of the sensor 1 and Cu2+ was 30 μM.
88x64mm (600 x 600 DPI)

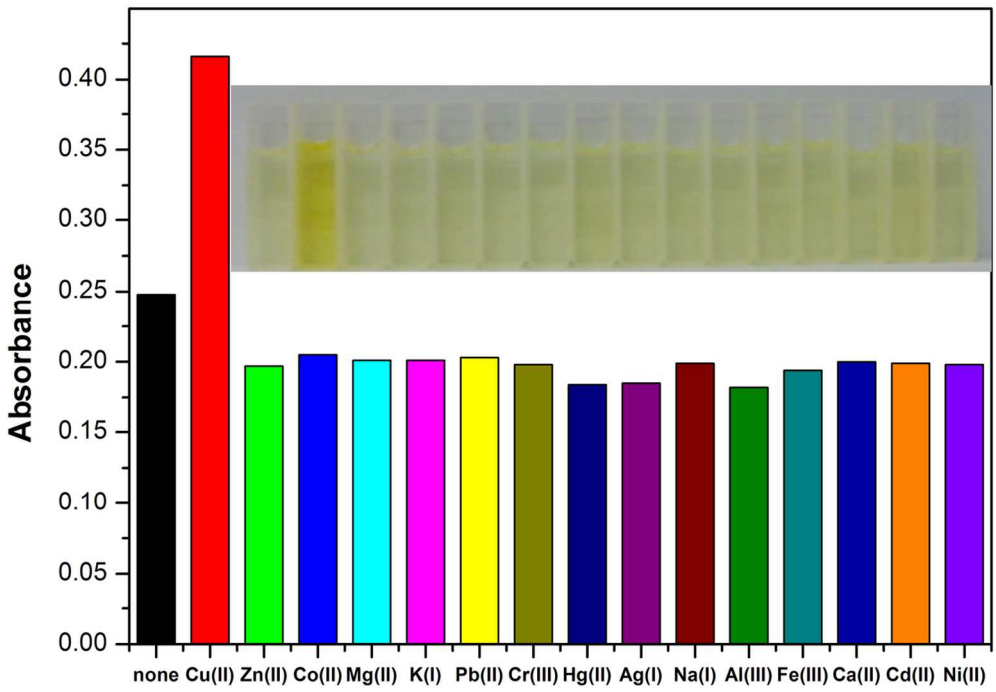

Fig. 5. Absorption changes of the sensor 1 (10 μM) upon addition of 3.0 equiv. of individual metal ions in 0.1 M HEPES-DMSO (9:1, v/v, pH = 7.2) solution; Inset: a picture of absorption changes of the sensor 1 (10 μM) upon addition of 3.0 equiv. of individual metal ions in 0.1 M HEPES-DMSO (9:1, v/v, pH = 7.2) solution.
118x82mm (300 x 300 DPI)

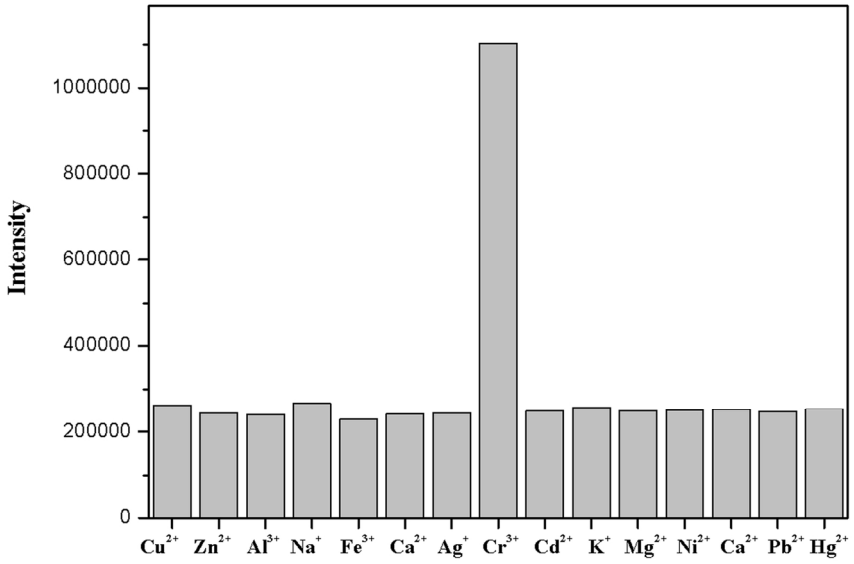

Fig. 6. Fluorescence response of the sensor 1 (10 μM) and Cu2+ (30 μM) in the presence of other different metal ions (30 μM) in 0.1 M HEPES-DMSO (9:1, v/v, pH = 7.2) solution.
79x52mm (600 x 600 DPI)

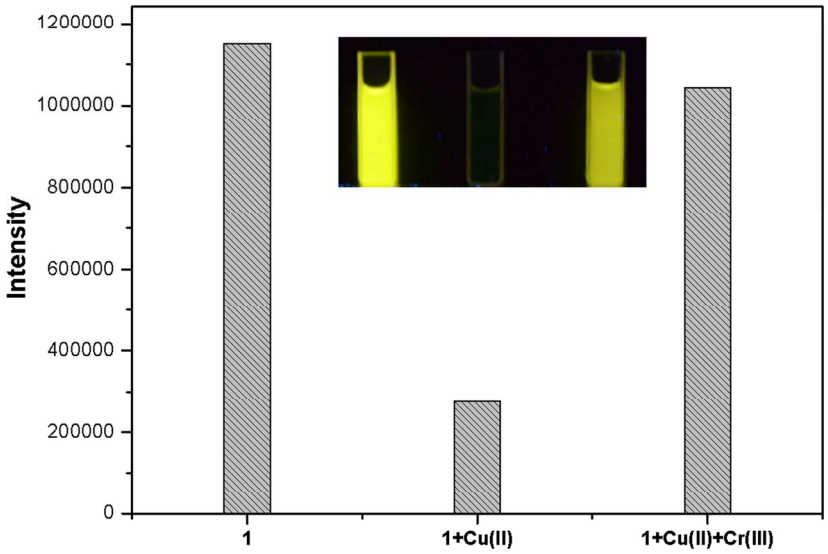

Fig. 7. Fluorescence response of the sensor 1 (10 μM) and Cu2+ (30 μM) in the presence of other different metal ions (30 μM) in 0.1 M HEPES-DMSO (9:1, v/v, pH = 7.2) solution.
77x50mm (600 x 600 DPI)

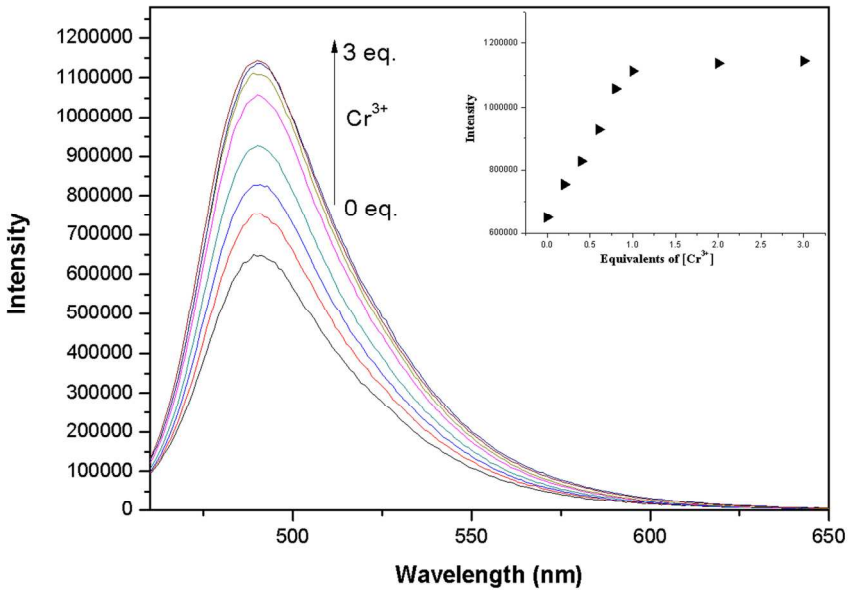

Fig. 8. Fluorescence changes of 1-Cu2+ (10 μM) on addition of different equivalents of Cr3+ in 0.1 M HEPES-DMSO (9:1, v/v, pH = 7.2) solution. Inset: the fluorescence intensity of 1-Cu2+ (10 μM) at 491 nm as a function of equivalents of Cr3+ in 0.1M HEPES-DMSO (9:1, v/v, pH = 7.2) solution.
80x53mm (600 x 600 DPI)

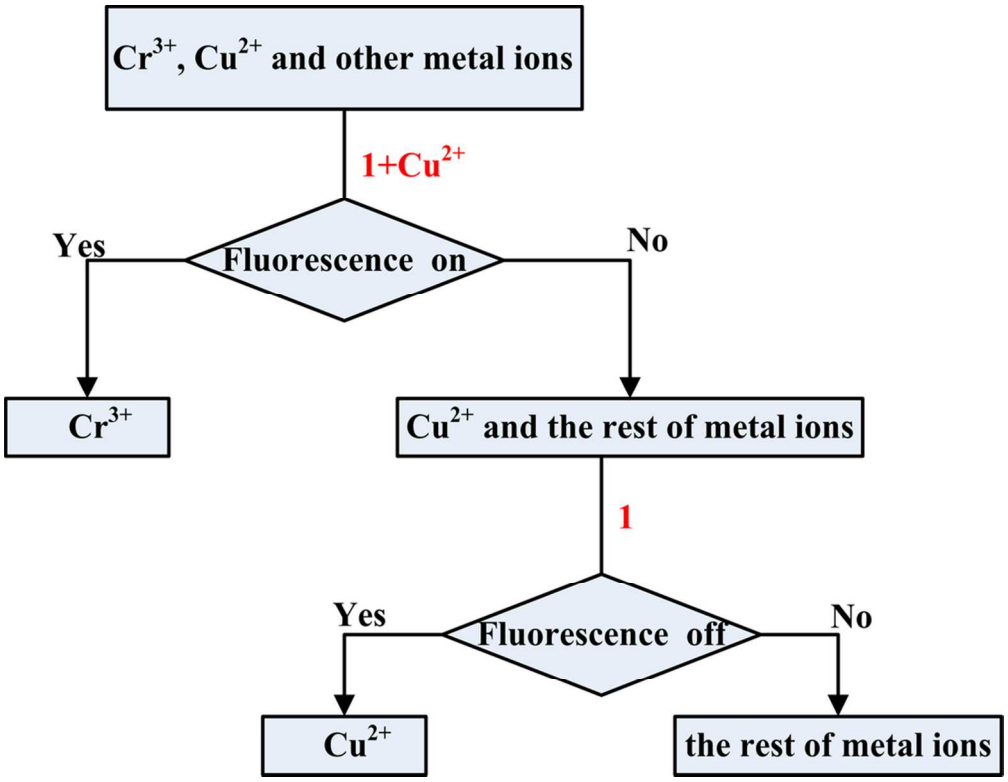

Scheme 2. Schematic for the analysis of the mixed metal ions using the sensor 1.
94x72mm (300 x 300 DPI)

Table 1. XPS results of the sensor **1** and **1**-Cu^{2+}.

Sample	1	1-Cu^{2+}	Coumarin 120	8-aminoquinoline	assignment
N1s(FWHM)	397.31(1.10)	396.76(1.01)	-	-	–HN*–C=O
	396.68(0.78)	396.49(0.92)	-	396.80(1.47)	aromatic N*
	396.06(0.94)	395.96(0.98)	396.19(1.08)	395.96(1.02)	*NH_2 or *NEt_2
O1s(FWHM)	530.95(1.58)	531.05(1.52)	530.89(1.72)	-	–O*–C=O
	529.36(1.55)	529.47(0.88)	-	-	–HN–C=O*
	528.33(1.52)	528.93(1.0)	528.39(1.24)	-	–O–C=O*
	--	529.66(1.89)	-	-	NO_3*

Asterisk (*) presents the assigned atom.

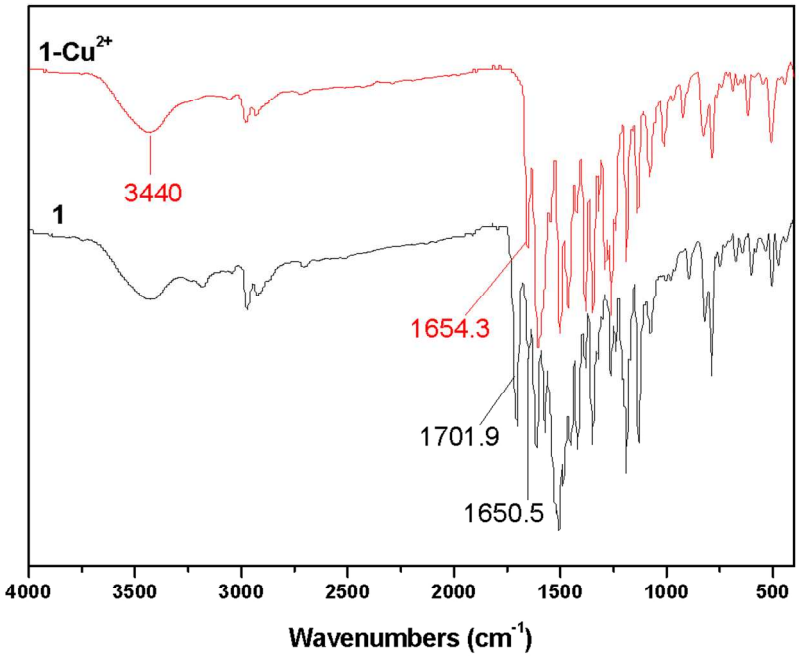

Fig. 9. FT-IR spectra of the sensor 1 and 1-Cu2+ with the KBR compression method.
93x72mm (600 x 600 DPI)

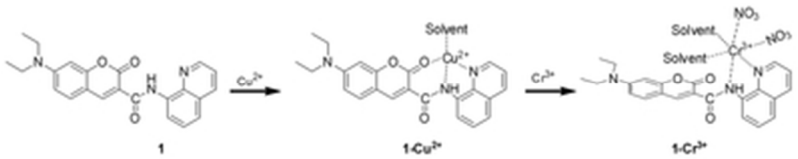

Fig. 10. Possible sensing mechanism of the sensor 1 for the sequential recognition of Cu2+ and Cr3+.
33x6mm (300 x 300 DPI)

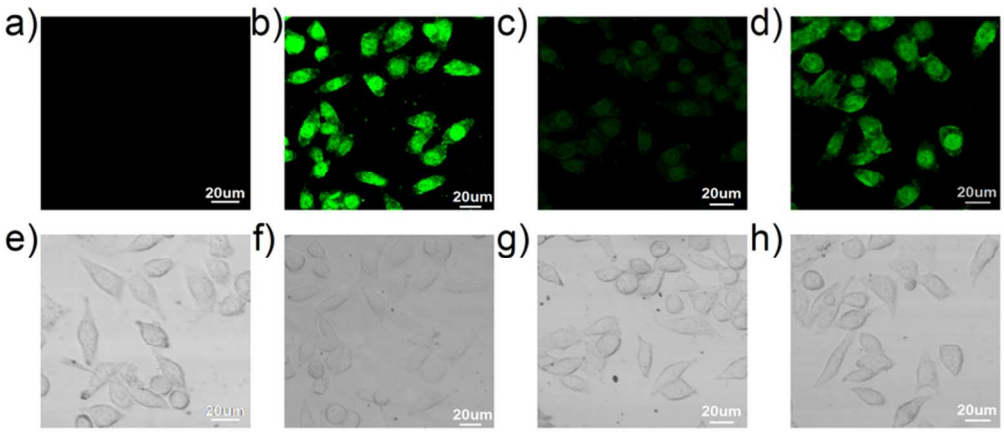

Fig.11. Confocal fluorescence images in MCF-7 cells. (a) cells untreated with any samples as blank test; (b) cells incubated with 10 μM of the sensor 1 for 30 min at 37 0C; (c) cells further incubated with 30 μM of the Cu2+ solution for another 30 min at 37 0C; (d) cells incubated with 10 μM of the sensor 1 and 30 μM of the Cu2+ solution, and further incubated with 30 μM of the Cr3+ solution for 30 min at 37 0C; (e) bright field image of cells in panel a; (f) bright field image of cells in panel b; (g) bright field image of cells in panel c; (h) bright field image of cells in panel d.
73x31mm (300 x 300 DPI)